PROTON BEAM ACCELERATION WITH CIRCULAR POLARIZED LASER PULSES*

X.Q. Yan[#], C.Lin , H.Y.Wang , Y.R. Lu, Z.Y. Guo, J.E. Chen,
State Key Lab of Nuclear Physics and Technology, IHIP,
Peking University, Beijing, China, 100871

Abstract

Recently, radiation pressure acceleration (RPA) has been proposed and extensively studied, which shows circularly polarized (CP) laser pulses can accelerate mono-energetic ion bunches in a phase-stable-acceleration (PSA) way from ultrathin foils. For appropriate parameters, CP pulses may accelerate foils as a whole with most of the transferred energy carried by ions. It is found that self-organizing proton beam can be stably accelerated to GeV in the interaction of a CP laser with a planar target at $\sim 10^{22} W/cm^2$. A prototype of laser proton accelerator (>10MeV) is going to be built at Peking University in the near future.

INTRODUCTION

State-of-the-art lasers can deliver ultraintense, ultrashort laser pulses, with intensities exceeding $10^{21} W/cm^2$, with very high contrast ratios, in excess of 10^{10}:1. These systems can avoid the formation of plasma by the prepulse, thus opening the way to laser-solid interactions with ultra-thin solid targets [1,2]. Solid targets irradiated by a short pulse laser can be an efficient and flexible source of MeV protons as well as highly charged MeV ions. Such proton beams are already applied to produce high-energy density matter [3] or to radiograph transient processes [4], and they offer promising prospects for tumor therapy [5], isotope generation for positron emission tomography [6], and fast ignition of fusion cores [7].

In the intense-laser interaction with solid foils, usually there are three groups of accelerated ions. The first two occur at the front surface, moving backward and forward, respectively, and the third one is sheath acceleration (TNSA) that occurs at the rear surface [8,9]. As these output beams are accelerated only by electrostatic fields and have no longitudinal bunching in (x, p_x) plane, their distribution profiles used to be exponential nearly with 100% energy spread. Although some techniques can be used to decreasing the energy spread, however, they rely on relatively complicated target fabrication [10~12]. Recently, radiation pressure acceleration (RPA) has been proposed and extensively studied, which shows ultra-intense laser pulses can accelerate mono-energetic ion bunches in a phase-stable-acceleration (PSA) way from ultrathin foils [13~20].

In these surface acceleration mechanisms, the linear polarized (LP) laser pulse is used and the J×B heating [13] is efficient to generate the hot electrons. For a

circularly polarized (CP) laser pulse with the electrical field $E_L = E(x)(\sin(\omega_L t)\hat{y} + \cos(\omega_L t)\hat{z})$, however, the ponderomotive force is $\vec{f}_p = -\frac{m_e c^2}{4}\frac{\partial}{\partial x}a_L^2(x)\hat{x}$ and its oscillating part vanishes. Here $a_L (x) = eE / m_e \omega_L c$ is the normalized laser amplitude, and m_e , ω_L and e are the electron mass, laser frequency and charge, respectively. When a CP laser is normally incident on a thin foil, the electrons are pushed forward steadily by the ponderomotive force. There is a regime of proton acceleration in the interaction of a CP laser with a thin foil in a certain parameter range, where the proton beam is synchronously accelerated and bunched like in a conventional RF linac. The acceleration mechanism is thus named as Phase Stable Acceleration (PSA). An analytic model is presented to show the acceleration and bunching processes duration the laser interaction.
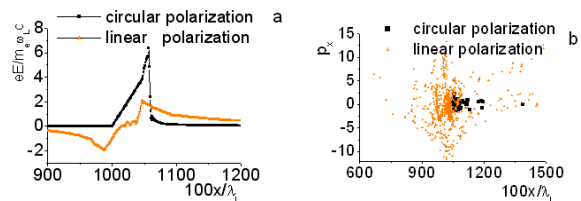

Figure 1: A thin solid-density target (n_0/n_c=10, D=0.2λ_L) is irradiated by a short laser pulse with a normalized laser amplitude $a_L = 5$. (a) Electrostatic field (b) Electron phase space (x, p_x) distribution.

As the oscillating part of the ponderomotive force is zero for CP laser pulse and J×B heating does not work, thus the interaction process is completely different from LP case. Fig.1 shows the electrical field profile and phase space projections for both circular and linear polarizations. In LP case, electrons are obvious heated by J×B force and randomly distributed in the space. The charge separation field is many times smaller than in CP case (see Fig.1a). In contrast, the electrons are quickly pushed inward by the ponderomotive force of the CP laser pulse, so that they pile up in the front of laser pulse and make up of a compressed electron layer.

PHASE STABLE ACCELERATION MODEL

In order to discuss the PSA regime easily, a simple model can been derived to elucidate the bunch formation for laser plasma interaction [16,23]. A linear profile of both in the electron depletion region ($E_{x1} = E_0 x / d$ for

$0 < x < d$) and in the compressed electron layer ($E_{x2} = E_0[1 - (x-d)/l_s]$ for $d < x < d+l_s$) (see Fig.2). The parameter E_0, n_{p0} and l_s are related by the equations $E_0 = 4\pi end$ and $n_{p0}l_s = nd \approx n_0 D$. As the E_{x1} increases with x, the protons starting at initial positions $x < d$ are debunched (longitudinally defocused) and their density will decrease in the electron depletion region. In contrary, because the E_{x2} decreases with x, the protons inside the compression layer ($d < x < d+l_s$) can be bunched by the electrostatic field E_{x2}. The equilibrium between the electrostatic and the ponderomotive forces on electrons is only transitorily lost and the electrons rearrange themselves quickly to provide a new equilibrium if the laser pulse is not over. So that the light pressure exerted on the electrons $(1+\eta)I_L/c$ is assumed to be balanced by the electrostatic pressure $E_0 en_{p0}l_s/2$. *Here η is the reflecting efficiency.*

As the purely hydrodynamic description isn't adequate to describe the interaction between the protons and electrons, dynamic equations are derived based on this model [23]. We introduce $\xi = (x_i - x_r)$ with $-l_s/2 \le \xi \le l_s/2$, where $x_r = d + l_s/2$ represents the position for the reference particle. The force acting on a test ion is given by $F_i = q_i E_0(1 - (x_i - d)/l_s)$. Thus, the motion equation for the proton is $\frac{d^2 x_i}{dt^2} = \frac{q_i E_0}{m_i \gamma^3}(1 - (x_i - d)/l_s)$, γ is the relativistic factor for reference particle. The phase motion (ξ, t) can be written as:

$$\ddot{\xi} = -\Omega^2 \xi, \Omega^2 = \frac{q_i E_0}{m_i l_s \gamma^3} \qquad (1)$$

For the reference ion γ varies slowly and E_0 is assumed to be quasi-constant the longitudinal phase motion (ξ, t) is a harmonic oscillation. We can obtain

$$\xi = \xi_0 \sin(\Omega t) \qquad (2)$$
$$\dot{\xi} = -\xi_0 \Omega \cos(\Omega t) \qquad (3)$$

If we take the laser amplitude a_L=5, n_0/n_c=10, and γ =1 for protons at the beginning, the period of the first longitudinal oscillation is about 8 T_L, which was consistent with simulation results as shown in Fig.4. If the final energy of reference particle w_r = 300 MeV, then energy spread $\Delta w/w_r = \xi_0 \Omega/w_r$ will be less than 4%.

PIC SIMULATIONS

In order to examine the present model and dynamics process, we carried out 1D simulations by a fully relativistic PIC simulation code (KLAP)[16,26] with 100 particles per cell per species, with cell sizes of $\lambda_L/100$. In PIC simulations a laser pulse with $a_L = 5$ and duration 100 T_L is incident on a purely hydrogen plasma

(cold, step boundary, overdense plasma slab with $n_0/n_c = \omega_p^2/\omega_L^2 = 10$ and $D = 0.2\lambda_L$) where $n_c = m_e \omega_L^2/4\pi e^2$ is the critical density, ω_p is the plasma frequency. In simulations the target boundary is located at $x = 10\lambda_L$ and the laser impinges on it at $t = 10 T_L$, λ_L and T_L are the laser wavelength and period. The a_L is the laser field amplitude given in units of the dimensionless parameter $a_L = eE_L/m_e \omega_L c$, m_e, ω_L and e are the electron mass, laser frequency and charge, respectively.
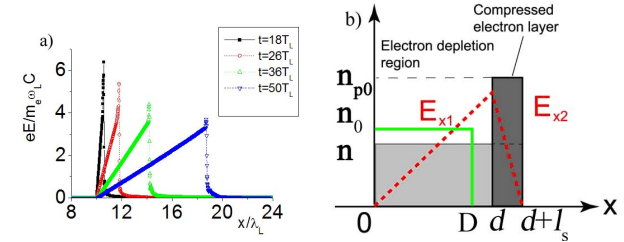

Figure 2: (color online) (a) Snapshots of the spatial distributions of the electrostatic fields at different time, where the initial plasma density $n_0/n_c = 10$ and thickness $D = 0.2\lambda_L$, normalized laser peak-amplitude $a_L = 5$ and pulse duration τ=100 T_L; (b) Schematic of the equilibrium density profiles for ions (n) and electrons (n_{p0}). The x position at x=d indicates the electron front, where the laser evanescence starts and it vanishes at x=d+ l_s, where l_s is the plasma skin depth. The initial plasma density n_0 and target thickness D are also plotted.
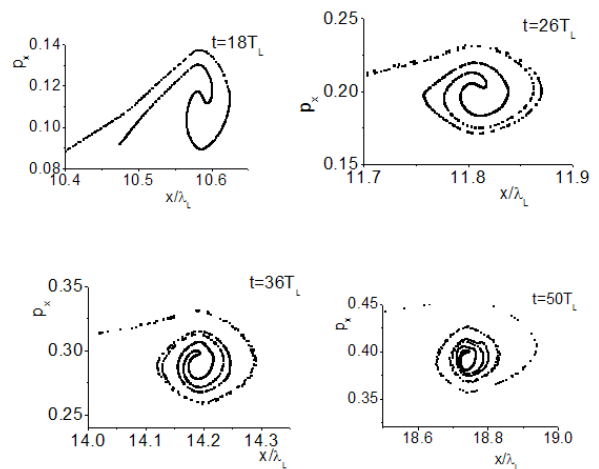

Figure 3: Evolution of phase space distribution for protons, the 1st, 2nd, 3rd and 4th oscillation period are 8, 8, 10 and 14 T_L respectively. The laser reflection efficiency $\eta = 0.38$.

The snapshots of the electrostatic field profile in Fig.2a shows the depletion region expands with time and the proton density in this region decreases, so that the slope of the field in the depletion region reduces gradually. In

the compressed electron layer, it is found that the width of the compression layer remains to be equal to the skin depth ($l_s \cong \lambda_L / 20$). Therefore the charge separation field in this layer nearly keeps the same steep linear profile, even though the maximum separation field is decreased slightly. It means the protons in the compressed electron layer can be synchronously accelerated and bunched by the charge separation field, so that the phase oscillations appear in the proton phase space (see Fig. 4), which is quite similar as in the radio frequency accelerator.
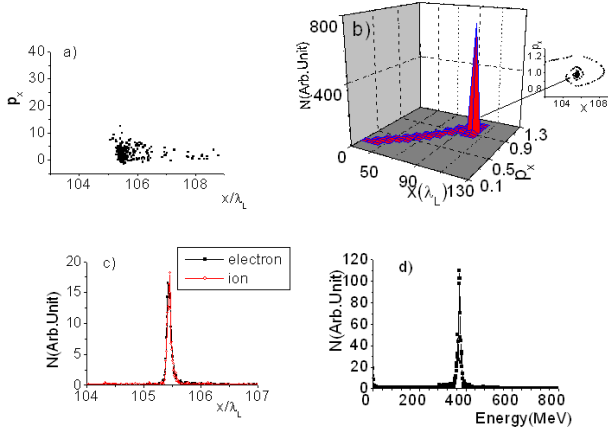

Figure 4: (color online) (a) Phase space distribution of electrons; (b) Phase space distribution of protons; (c) Electrons and protons density profiles; (d) Energy spectrum of protons. The results are found at t=200 T_L when the laser interaction is almost terminated. The laser and plasma parameters are the same as in Fig. 1.
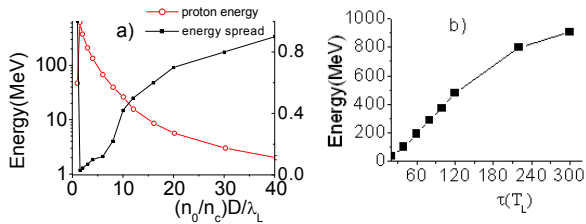

Figure 5: (a) Proton energy of the mono-energetic peak versus target thickness and density for a_L=5 and laser pulse duration τ=100 T_L; (b) Proton energy of the mono-energetic peak versus laser pulse duration for a_L=5, $n_0 / n_c = 10$, and D=0.2λ_L.

The snapshots of phase-space distributions of electrons and ions at t=200 T_L are plotted in Fig. 4(a) and Fig. 4(b). It shows a bunched proton beam with a very high density is formed in the phase space (x,p_x), because protons inside the compressed electron layer always execute periodical oscillations as described by Eq. (3). The protons in the electron depletion region (between x=0 and 100) are debunched and form a long tail in the phase space, however, its density is two-orders lower than in the compressed electron layer. As a result, the debunched protons look disappearing in the proton spatial distribution and the proton energy spectrum, which are shown in Fig. 4(c) and Fig. 4(d), respectively. Fig. 4(c)

implies both particles have the same density profiles and a quasi-neutral beam is therefore obtained. In this case, the space charge fields are weak and the proton beam can propagate over a long distance without explosion, which is advantageous to transport the high current ion beams in applications. The energetic proton beam has a low FWHM energy spread (< 4%) and high peak current as shown in Fig. 4(d). The energy spread is completely in agreement with our earlier estimation based upon Eq. (3). Note that the proton bunch has an ultrashort length about the skin depth l_s or about 250 attoseconds in time (λ_L=800 nm). The number of accelerated protons in the bunch is about $n_0 l_s \sigma$, where σ is the focused beam spot area. This gives about 5×10^{12} quasi-monoenergetic protons for a focused beam diameter of 40μm in the present simulation.

In 1D simulations it is found that the proton energy depends on the product of target density and thickness. The proton energy and the energy spread are plotted versus the electron area density in Fig. 5(a). It shows that the energy spread can be optimized near the condition $a_L \sim (n_0 / n_c) D / \lambda_L$. Figure 5(b) suggests that the proton energy increases almost linearly with the laser pulse duration at first, Later it turns to be saturated because the protons become relativistic.
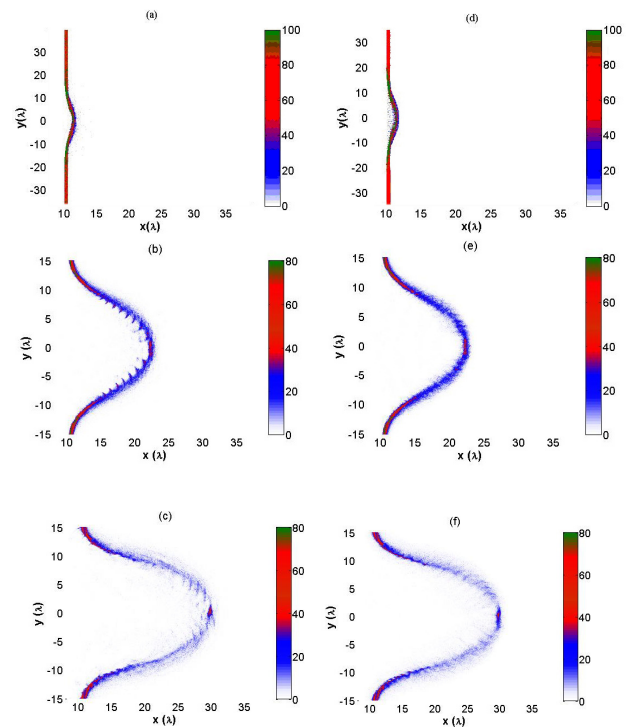

Figure. 6 (color online): Foil density evolution. Left: electrons, right: ions, at times (a,d) $t = 16$, (b,e) $t = 36$, (c,f) $t = 46$, in units of laser period. The laser pulse is incident from the left and hits the plasma at $t = 10$. Only half the transverse size of the simulation box is plotted in frames b, c, e, f for better resolution of fine structures. Here $a_L = 50$ and pulse duration is 30T_L.

For appropriate parameters, CP pulses may accelerate foils as a whole with most of the transferred energy carried by ions. The basic dynamics are well described by a one-dimensional (1D) PSA model. Acceleration terminates due to multi-dimensional effects such as transverse expansion of the accelerated ion bunch and transverse instabilities. In particular, instabilities grow in the wings of the indented foil, where light is obliquely incident and strong electron heating sets in. Eventually, this part of the foil is diluted and becomes transparent to the driving laser light. The central new observation in the present paper is that this process of foil dispersion may stop before reaching the centre of the focal spot and that a relatively stable ion clump forms near the laser axis which is efficiently accelerated. The dense clump is about 1 - 2 laser wavelengths in diameter. The stabilization is related to the driving laser pulse that has passed the dispersed foil in the transparent wing region and starts to encompass the opaque clump, keeping it together.

Figure 7 highlights the central results concerning clump evolution. The total number of protons, comprised within a $\lambda/2$ distance from the laser axis and shown in Fig. 7a, drops after time $t = 26$ from an initial value of 2.5×10^{10} due to transverse expansion, but this trend is interrupted at about $t = 35$, when the foil becomes transparent in the wing region and the new regime of quasi-stable acceleration sets in. In the present 2D-PIC simulation, about 1.7×10^{10} protons (1 nano-Coulomb) are trapped in the central clump and are accelerated to an ion energy of approximately 1 GeV. The ion energy spectra exhibit sharp peaks, as it is seen in Fig. 7b.
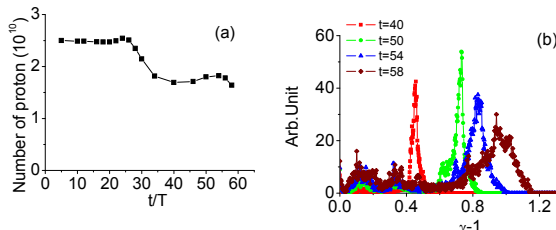

Figure 7: (color online):(a) Number of protons in the center of the foil ($r \le \lambda$) versus time in units of laser cycles; (b) evolution of energy spectrum for beam ions located inside the central clump ($r \le \lambda$).

Maximum proton energy versus laser intensity is plotted in Figure 8. The black squares represent results from the 2D-PIC simulations described below, they follow an effective scaling of $I^{0.8}$.
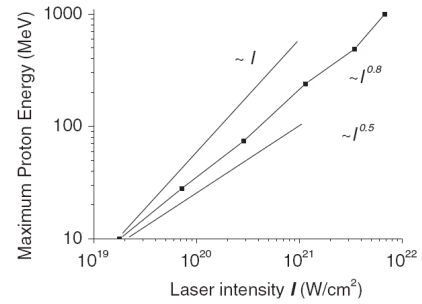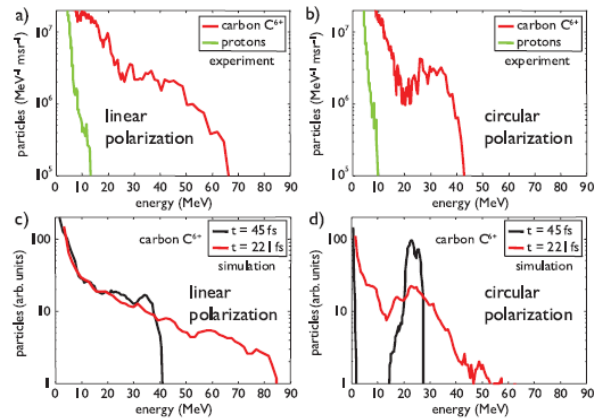

Figure 8: Proton energy versus laser intensity.

Figure 9: Experimentally observed proton (green curves). and carbon C^{6+} (red curves) spectra in the case of linear (a) and circular (b) polarized irradiation of a 5.3 nm thickness DLC foil. The corresponding curves as obtained from 2D PIC simulations (c),(d) show excellent agreement with the measured distributions at late times.

PROOF OF PRINCIPLE EXPERIMENT [24]

There was successful experimental demonstration on ion acceleration from ultrathin diamond-like carbon foils (DLC) irradiated by ultrahigh contrast laser pulses of energy 0.7 J focused to peak intensities of 5×10^{19} W/cm^2[24]. A reduction in electron heating is observed when the laser polarization is changed from linear to circular, leading to a pronounced peak in the fully ionized carbon spectrum at the optimum foil thickness of 5.3 nm as shown in Fig. 9. Two-dimensional particle-in-cell simulations reveal that those C^{6+} ions are for the first time dominantly accelerated in a phase-stable way by the laser radiation pressure.

LASER PLASMA LENS [25]

In principle higher proton energy (for example: GeV) can be realized by using a higher laser intensity, however, the acceleration will be terminated soon due to hole-boring effects and transverse instabilities [15,16,17,18]. In order to accelerate ions to a relativistic velocity, normally extremely high laser intensity ($>10^{21} W/cm^2$), sharp rising front, and high temporal laser contrast ($>10^{10}$) are required, which are very challenging for state of art

laser technology. We propose a plasma lens to make high intensity, high contrast laser pulses with a steep front. When an intense, short Gaussian laser pulse pass through nearly critical dense plasma, the laser pulse will be compressed and focused into a channel due to self-focusing and self-modulation. If it is used as a plasma lens, Fig. 10 shows clearly three pulse shaping effects are realized synchronously: I) pulse focusing that results in laser intensity enhancement; II) laser profile steepening; III) absorption of non-relativistic prepulse. The transmission efficiency of the lens can be as high as 60% and it will be useful for many applications such as generation of high-energy ions and electrons.
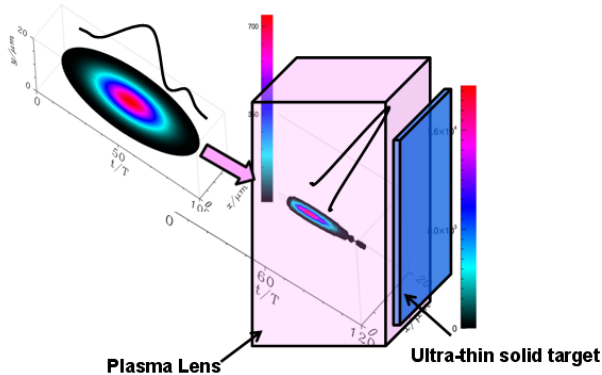

Figure 10: Laser plasma lens for pulse shaping and cleaning.

FUTURE PLAN AT PEKING UNIVERSITY

A prototype of laser driven proton accelerator (10~100MeV) based on the PSA mechanism [16,22,23] and plasma lens [25] will be built at Peking University in the upcoming few years. It will be used for the applications such as cancer therapy, plasma imaging and fast ignition for inertial confine fusion.
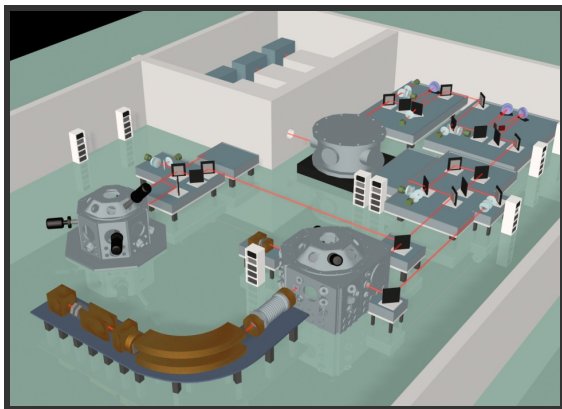

Figure 11: LAser Proton Accelerator (LAPA) at Peking University.

ACKNOWLEDGMENT

REFERENCES

[1] G. A. Mourou, T. Tajima, and S. V. Bulanov, Rev. Mod. Phys. 78, 309 (2006).

[2] A. J. Machinnon et al, Phy.Rev.Lett.88, 215006 (2002).

[3] P. Patel et al., Phys. Rev. Lett. 91, 125004 (2003).

[4] M. Borghesi et al., Phys. Plasmas 9, 2214 (2002).

[5] S. V. Bulanov, T. Zh. Esirkepov, V. S. Khoroshkov, A. V. Kuznetsov, F. Pegoraro, Phys. Lett. A 299, 240 (2002).

[6] I. Spencer et al., Nucl. Inst. Meth. Phys. Res. B 183, 449 (2001).

[7] M. Roth et al., Phys. Rev. Lett. 86, 436 (2001).

[8] P. Mora, Phys. Rev. Lett. 90, 185002 (2003); T. Esirkepov, M.Yamagiwa, and T.Tajima Phys. Rev. Lett. 96, 105001 (2006).

[9] Y. T. Li, Z. M. Sheng et al, Phy. Rev. E 72, 066404 (2005).

[10] H. Schwoerer et al., Nature 439, 445 (2006).

[11] T. Toncian et al., Science 312, 410 (2006).

[12] M.Hegelich et al, Nature 439, 441 (2006).

[13] W. L. Kruer, et al, Phy.Fluids 28, 430 (1985).

[14] A. Macchi, F. Cattani, T.V. Liseykina, F. Cornolti, Phys. Rev. Lett. 94, 165003 (2005); S.G. Rykovanov, J. Schreiber, J. Meyer-ter-Vehn, C Bellei, A. Henig, H.C. Wu and M. Geissler, New J. Phys. 10, 113005 (2008) ; X. Zhang, et al., Phys. Plasmas 14, 123108 (2007); C.S. Liu, V.K. Tripathi and X. Shao, Frontiers in Modern Plasma Physics 246-254 (2008).

[15] O. Klimo, J. Psikal, and J. Limpouch, and V. T. Tikhonchuk, Phys. Rev. Special Topics - Accelerators and Beams 11, 031301 (2008).

[16] X.Q.Yan et al., Phys. Rev. Lett. 100, 135003 (2008).

[17] A. P. L. Robinson, M. Zepf, S. Kar, R.G. Evans, and C. Bellei, New J. Phys. 10, 013021 (2008).

[18] M. Chen, A. Pukhov, Z.M. Sheng, X.Q.Yan, Physics of Plasma, 15, 113103 (2008).

[19] Y. Yin, W. Yu, M. Y. Yu, A. Lei, X.Yang, H. Xu and V.K. Senecha, Phys. Plasmas 15, 093106 (2008).

[20] T. Esirkepov, M. Borghesi, S. V. Bulanov, G. Mourou, and T. Tajima, Phys. Rev. Lett. 92, 175003 (2004).

[21] X. Q. Yan, et al.,Phys. Rev. Lett. 103, 135001 (2009)

[22] X. Q. Yan, et al., Physics of Plasmas 16, 044501, (2009).

[23] B. C. Liu, et al., IEEE Transactions On Plasma Science, Volume 36, Issue 4, 1854 – 1856 (2008).

[24] A. Henig, et al., Phys. Rev. Lett. 103, 245003 (2009).

[25] H.Y.Wang, et al., Phys. Rev. Lett. 107, 265002 (2011).

[26] Z. M. Sheng, et al., Phys. Rev. Lett. 94, 095003 (2005).